pH-Dependent Photoisomerization of Retinal in Proteorhodopsin†

Robert Huber,‡ Thomas Köhler,‡ Martin O. Lenz,‡ Ernst Bamberg,§ Rolf Kalmbach,|| Martin Engelhard,|| and Josef Wachtveitl*,‡

Institut für Physikalische und Theoretische Chemie, Marie-Curie-Strasse 11, Johann Wolfgang Goethe-Universität Frankfurt, 60439 Frankfurt am Main, Germany, Max-Planck-Institute of Biophysics, Department of Biophysical Chemistry, Marie-Curie-Strasse 15, 60439 Frankfurt am Main, Germany, and Max-Planck-Institute of Molecular Physiology, Department of Physical Biochemistry, Otto-Hahn-Strasse 11, 44227 Dortmund, Germany

Received August 5, 2004; Revised Manuscript Received October 12, 2004

ABSTRACT: The early steps in the photocycle of the bacterial proton pump proteorhodopsin (PR) were analyzed by ultrafast pump/probe spectroscopy to compare the rate of retinal isomerization at alkaline and acidic pH values. At pH 9, the functionally important primary proton acceptor (Asp97, pK_a = 7.7) is negatively charged; consequently, a reaction cycle analogous to the archaeal bacteriorhodopsin (BR) is observed. The excited electronic state of PR displays a pronounced biphasic decay with time constants of 400 fs and 8 ps. At pH 6 where Asp97 is protonated a similar biphasic decay is observed, although it is significantly slower (700 fs and 15 ps). The results indicate, in agreement to similar findings in other retinal proteins, that also in PR the charge distribution within the chromophore binding pocket is a major determinant for the rate and the efficiency of the primary reaction.

Since the membrane protein proteorhodopsin (PR)[1] as a new member of the type I retinal binding protein family (with bacteriorhodopsin (BR) as a prominent member) was discovered in uncultivated marine γ-proteobacteria interest has arisen because of its potential relevance for a new principle of phototrophic growth in the ocean's photic zone (*1*, *2*). After the discovery of PR, a wide variety of homologous sequences in marine planktonic bacteria from different locations have been identified (*3*−*5*). PR, just like BR, was shown to work as an outward directed light-driven proton pump, resulting in a proton gradient across the membrane which might be used by γ-proteobacteria for their energy requirements such as ATP synthesis.

After light excitation, PR undergoes a photocycle whose sequence of intermediates is similar to that of the BR photocycle and has been denoted accordingly K, M, N, and O (*6*−*10*). Although the turnover time is slightly slower to that of BR, it is considerably faster than that typical for sensory photoreceptors such as sensory rhodopsins I and II (SR I, SR II) (*11*). It was therefore assumed that PR is likely to be a proton pump, but not a sensor.

Thus, BR can be regarded as a model system for PR which is also exemplified in the sequence homology of those amino acids involved in the vectorial proton transfer. Residues characteristic for the cytoplasmatic and the extracellular channel are conserved as well as two-thirds of the residues forming the retinal binding pocket (*12*). The latter amino acids include the primary proton acceptor Asp97 (Asp85 in BR), and components of the complex counterion of the protonated Schiff base, Arg94 and Asp227 (Arg82 and Asp212 of BR) (*8*). The primary proton donor Asp96 in BR is replaced by Glu108 in PR (*1*). Although BR and PR share many homologous amino acids participating in proton transport, PR probably lacks some ionizable residues at the cytoplasmic side, which in BR are involved in fast proton release (*1*, *13*−*15*).

Remarkably, PR contrary to BR was shown to reverse the direction of proton transport at pH values below the pK_a of Asp97 (pK_a = 7.7). The data were obtained from pH-dependent photocurrent measurements of PR (*7*). It should be noted that an inversion of the proton was not seen in experiments using photoelectric current measurements on oriented membrane fragments (*16*).

The photoisomerization of the retinal is, as in all other rhodopsin-like proteins, the key event of the PR photocycle. Light-adapted PR contains 40% 13-*cis* and 60% *all-trans* retinal PR, a ratio that is shifted to 20/80 in dark-adapted PR. The acidic form of PR displays no difference between the light- and the dark-adapted state; the ratio of *cis*/*trans* is 20/80 for both cases (*7*). At alkaline pH values, retinal isomerization from *all-trans* to 13-*cis* causes deprotonation of the Schiff-base and proton uptake by Asp97. The formation of a blue-shifted M-like intermediate, indicative for the deprotonated Schiff base, is observed on the microsecond time scale (*6*−*9*).

Numerous publications discuss the earliest photoevents in BR, addressing the very fast molecular motions and the rate of the *all-trans* → 13-*cis* isomerization of retinal. This first

† This work was supported partly by the Deutsche Forschungsgemeinschaft, SFB 472 (to T.K., M.O.L., E.B., and J.W.).

* To whom correspondence should be addressed. Tel.: +49 (0)69 798 29351. Fax: +49 (0)69 798 29709. E-mail: wveitl@theochem.uni-frankfurt.de.

‡ Johann Wolfgang Goethe-Universität Frankfurt.

§ Max-Planck-Institute of Biophysics.

|| Max-Planck-Institute of Molecular Physiology.

[1] Abbreviations: PR, proteorhodopsin; BR, bacteriorhodopsin; SR I, sensory rhodopsin I; SR II, sensory rhodopsin II; HR, halorhodopsin; J, K, M, N, and O, intermediates of the photocycle; DM, dodecylmaltoside; PBS, phosphate-buffered saline; CMC, critical micellar concentration; FC, Franck−Condon region; CI, conical intersection.

10.1021/bi048318h CCC: $30.25
Published on Web 01/15/2005

part of the photocycle ranges from the photoexcitation of BR to the formation of the K intermediate, which is completed after 3.5 ps (*11*, *17*−*23*). A generally accepted description includes the following reaction steps: Upon photoexition the *all-trans* retinal reaches the first exited electronic-state (S_1) with ionic (B_u-like) character. Propagation on the multidimensional potential energy surface S_1 involves a retinal stretching mode, before the torsional motion around C13−C14 double bond starts. The path terminates at a S_1/S_0 conical intersection (i.e., the molecule relaxes radiationless to the electronic ground-state S_0) at an approximately 90° twisted geometry (*22*, *23*). Back at the S_0 potential surface the path splits: the molecule either adopts an *all-trans* configuration or a 13-*cis* configuration. The latter is termed the spectroscopic K intermediate in the photocycle.

The spectroscopic characteristics of retinal and the dynamics of the isomerization are highly dependent on its molecular surroundings. Various retinal proteins have been shown to modulate the primary photoreaction and absorption characteristics (spectral tuning) according to different biological requirements (*24*, *25*). The electronic configuration of the chromophore is highly dependent on the electrostatic potential of the residues in the protein (especially the complex counterion to the Schiff-base) and the geometry of the chromophore (*26*−*28*). The major factors within the protein microenvironment that influence the photophysical properties of the retinal are subject to intense investigations but are still only partially understood.

The absorption maximum of PR is known to exhibit a red shift when the pH is lowered (purple-to-red transition). This has been attributed to the protonation state of the primary proton acceptor Asp97 (*16*). As long as no structural information on PR is available, a BR-based molecular model has to support structural considerations regarding the Schiff base region of PR (*29*). Accordingly, Asp97 and Asp227, members of the complex counterion, are located closely to the protonated Schiff base. The pK_a of the Schiff base has been determined at 11.3, and considerable protonation of Asp227 may not occur above pH 5 (*30*). Between those values, electrostatic conditions at the Schiff base region are likely to be controlled by the protonation state of Asp97.

Here, the pH-dependent photoreaction of PR with a focus on the electrostatic control of the retinal isomerization is presented. Transient absorption experiments in the visible spectral range with femtosecond time resolution have been performed on PR samples at acidic and alkaline pH. The method provides information about electronic relaxation of the chromophore and the earliest intermediates of the PR photocycle. A comparison of the datasets demonstrates similar kinetic pathways but different velocities of the retinal isomerization for both PR samples.

MATERIALS AND METHODS

Sample Preparation. Expression and purification of PR in *Escherichia coli* membranes was performed as described in ref *7*. Purified PR was reconstituted in 25 M excess of polar lipids from purple membrane. Reconstitution was carried out in 1 M NaCl, 50 mM $NaPO_4$ (pH 8). The solubilized protein was diluted twice under CMC of 0.002% dodecylmaltoside (DM), and the remaining detergent was removed via detergent absorber beads (Boehringer, Mannheim) overnight at 4 °C. Acidic and alkaline pH values were adjusted by centrifugation (100000*g*) of the reconstituted protein and resuspension in PBS buffer with the corresponding pH.

Stationary Spectroscopy. Absorption spectra were recorded using a Hitachi spectrophotometer (model U-3000). Aliquots of the described samples were diluted with adequate buffers by a factor of 10 and measured in 1-mm path length fused silica cuvettes. Absorbance due to light scattering was approximated by a power function $A + B/\lambda^C$.

Transient Spectroscopy. In the following chapter, fs-time-resolved transient absorption measurements of PR at different pH values are presented. The experimental setup was based on a femtosecond pump/probe principle using a Clark CPA 2001 at a repetition rate of ≈1 kHz at a central wavelength of 775 nm. The laser served as pulse source for the following nonlinear processes. The excitation pulses were generated with a noncollinear optical parametric amplifier (NOPA) centered at a wavelength of 520 nm and focused to a diameter of 100 μm inside the sample. The pulse length was about 100 fs, and typical pulse energies were around 75 nJ, low enough to prevent multiphoton excitation of the sample. The sample was probed with single filament white light pulses generated in a CaF_2 plate (supercontinuum, polarization parallel to excitation pulse), a spectral range of 380−730 nm was selected for probing. Because of group velocity mismatch between pump and probe light, the temporal resolution of the system is wavelength dependent, and the cross correlation width for the entire investigated spectral range was between 70 and 120 fs. The continuum pulses were dispersed by two spectrometers (sample and reference), and recorded with two 42 segment diode arrays (multichannel detection), resulting in a spectral resolution of 8 nm. Data acquisition was performed in single shot detection mode as balanced and referenced measurement providing signal-to-noise ratios up to 10^4.

A continuous exchange of the sample between successive laser shots was achieved by using a flow cuvette (optical path length 500 μm) and a syringe pump. This prevents multiple excitation of molecules within the photocycle and accumulation of photoproducts.

Before further analysis, the data were corrected for the coherent signals and group velocity dispersion (GVD). With a procedure described by Kovalenko et al. (*31*), which uses the temporal evolution of the coherent signal and a least-squares fit algorithm, the delay time zero could be determined for all wavelengths. Data were then analyzed using a Marquardt downhill algorithm that allowed optimization of *n* exponential decays for all wavelengths simultaneously, while the amplitudes for each kinetic component are wavelength-dependent fitting parameters.

RESULTS

Stationary Spectroscopy, Sample Characterization. In the UV/vis spectrum of reconstituted PR (Figure 1) a pH-dependent shift of the absorption maximum of the major chromophore band from 521 nm (pH 9) to 536 nm (pH 6) can be observed. Additionally, the protein band at 280 nm and a minor band at 374 nm that is assigned to the β-band of the chromophore can be seen (*32*). As described in the methods section, the contribution from light scattering was

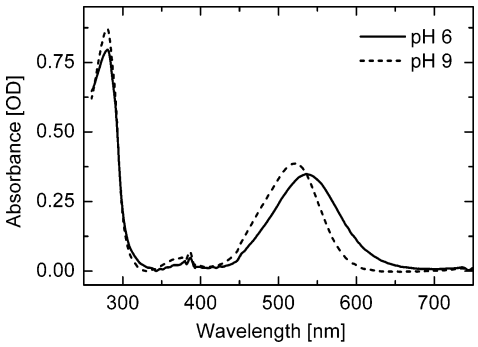

FIGURE 1: Absorption spectra of PR at acidic and alkaline pH. The absorption maximum shifts from 536 nm (PR^{acidic}) to 521 nm ($PR^{alkaline}$). For comparison to the femtosecond measurements, the spectra have been scaled to an OD corresponding to an optical path length of 500 μm. The spectra have been corrected for scattered light. See text for details.

approximated by a power function and subtracted from the data. The fitting procedure results in a value of $C \approx 2.5$ for both samples. Since reconstituted PR forms particles with diameters on the micrometer scale in this sample preparation, scattering is not only due to Rayleigh light scattering, which explains the deviation from the ω^4 dependence.

Transient Spectroscopy. For an overview of the temporal evolution, Figure 2 gives a color-coded illustration of the transient absorbance changes upon photoexcitation for PR at acidic and alkaline pH values. The plots are composed of up to 40 individual channels each and cover a spectral range from 427 to 723 nm at pH 6 and from 411 to 731 nm at pH 9. Red indicates positive, green indicates zero, and blue indicates negative absorbance changes. Because of the strong scattering of the sample the highlighted data around the excitation wavelength at 520 nm show higher noise amplitudes and will not be considered in the subsequent discussion. The transient absorbance spectra at pH 6 and pH 9 have several spectral features in common: centered around 450 nm, a dominant positive (yellow to red) transient absorbance can be identified for both samples. This signature arises after photoexcitation and reaches its maximum approximately 200 fs after delay time zero. At pH 6, the maximum is at about 460 nm, while the peak at pH 9 appears blue shifted at approximately 450 nm. The overall decay of the signal under alkaline conditions is faster than under acidic conditions. Figure 3a shows representative transient absorbance curves from this spectral region for both pH values. Upon excitation, an early absorption increase is observed, which decays on the picosecond time scale. At pH 6, the signal turns negative after approximately 10 ps and remains at a constant negative level up to 1 ns delay time. The transient absorbance changes at pH 9 show very similar characteristics but turn negative after 2 ps. A global fit analysis suggests two time constants to be involved in both kinetics: At pH 6 the signal decay can be described by the time constants $\tau_{2(pH6)} = 0.7$ ps and $\tau_{3(pH6)} = 15$ ps, and at pH 9 the kinetics are faster with $\tau_{2(pH9)} = 0.4$ ps and $\tau_{3(pH9)} = 8$ ps. Amplitude spectra related to the different decay times are shown in Figure 4.

At the red most end of the probed spectral range, i.e., for $\lambda_{pr} > 690$ nm, both PR samples exhibit negative contributions (Figure 2). After a dominant fast decay on the sub-picosecond time scale the signal disappears completely within approximately 30 ps for pH 6 and 2 ps for pH 9, which can be

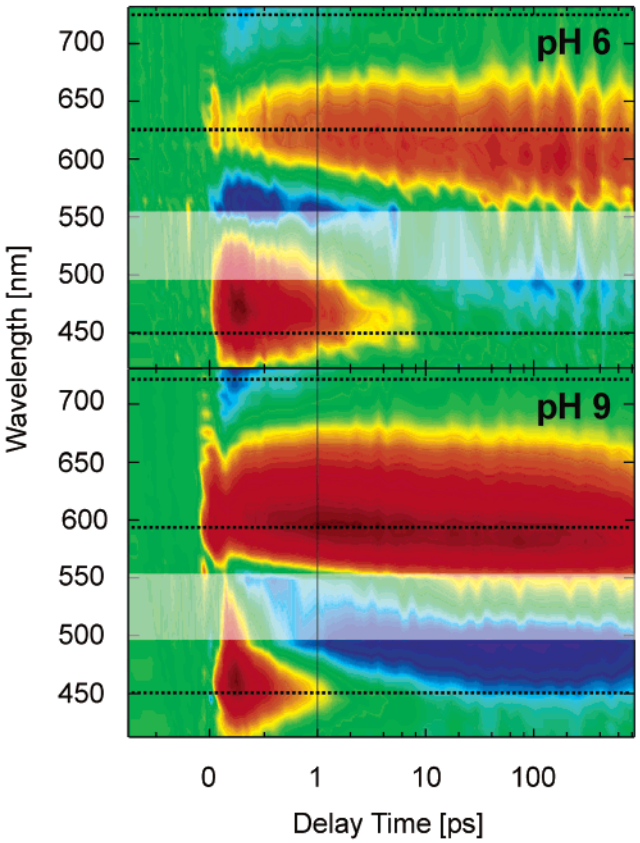

FIGURE 2: Temporal evolution of light/dark difference absorption of PR at pH 6 and 9 after excitation with a 520 nm pulse (multichannel detection). Signal amplitudes are color coded: red indicates positive, and blue negative absorbance change. Data around the excitation wavelength with a lower signal-to-noise ratio are plotted with less intense color code. A linear time scale is used for $\tau < 1$ ps, and a logarithmic one is used for longer delay times. Dotted lines represent the spectral positions of the transients selected for Figure 3.

clearly seen in the corresponding absorption transients of this region (Figure 3c). The results of the global fit analysis (see Figure 4) propose that the kinetics of this feature proceed with the same two time constants as mentioned above (pH 6: $\tau_{2(pH6)} = 0.7$ ps and $\tau_{3(pH6)} = 15$ ps, pH 9: $\tau_{2(pH9)} = 0.4$ ps and $\tau_{3(pH9)} = 8$ ps).

The most prominent positive transient absorbance centered at 600 nm persists at least until 1 ns. At pH 6, the maximal amplitude after 1 ps is reached at about 610 nm, and for pH 9 at 590 nm. For longer delay times, the maxima are blue shifted (pH 6: 600 nm; pH 9: 570 nm). A comparison of selected transients of this spectral region is given in Figure 3b and shows that for both samples two different features can be identified: (i) a rapid increase of absorption, which reaches its maximum at delay time zero and decays within 200 fs. This feature is more prominent at pH 9 than at pH 6. (ii) a persistent positive absorption that reaches its maximum after 5 ps (pH 6) and after 2 ps (pH 9), respectively. In both cases, a slow decrease of the signal amplitude is observed; nevertheless, a dominant fraction of positive absorption remains up to 1 ns. Amplitude spectra (Figure 4) show the individual contributions of the time constants τ_2 and τ_3 involved in that spectral region for both samples. While the fast component τ_2 indicates signal growth, the slower one turns positive around 650 nm, corresponding to signal decay.

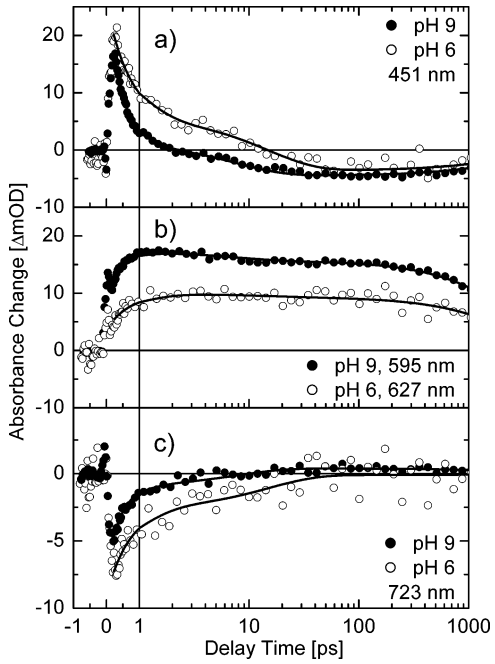

FIGURE 3: Comparison of transient absorbance changes of PR at acidic and alkaline pH at different probing wavelengths (dots). Solid lines represent results (for $\tau > 200$ fs) of a multiexponetial global fit analysis of the complete data sets.

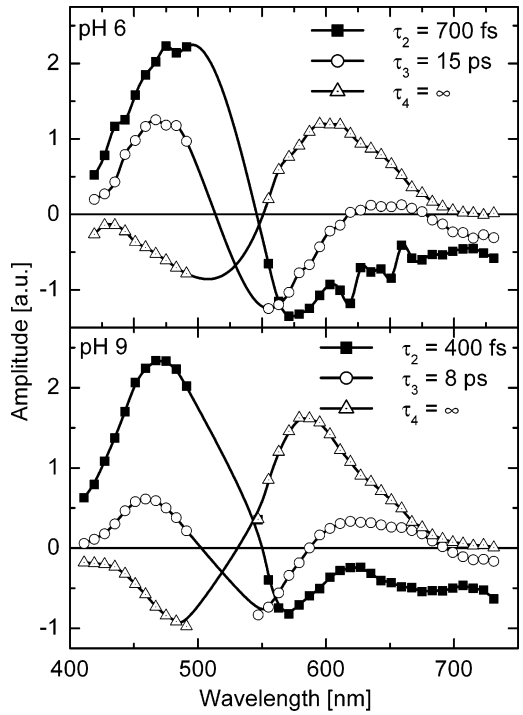

FIGURE 4: Amplitude spectra of the multiexponential global fit analysis of PR at pH 6 and pH 9. Data between 500 and 550 nm (corresponding to the fainter areas in Figure 2) are not considered in the data analysis.

Apart from the emission band around 700 nm, negative transient absorbance due to ground-state bleaching emerges near the excitation wavelengths in the spectra for both samples (Figure 2). The instantaneous bleach signal is obscured by different absorbing species during the picosecond-part of the PR photocycle. Thus, for PR at pH 6 the signatures can be unambiguously detected between 550 to 600 nm at delay times from 0 to 10 ps and later between 450 and 500 nm at delay times from 10 to 1000 ps. At pH 9 negative transient absorbance is observed between 450 and 500 nm at delay times from 1 to 1000 ps.

Table 1: pH-Dependent Time Constants of the Early Steps of the PR Photocycle

	τ_1 [ps]	τ_2 [ps]	τ_3 [ps]	τ_4 [ps]
PR (pH 6)	<0.2	0.7	15	>1000
PR (pH 9)	<0.2	0.4	8	>1000

Four time constants describe the datasets for both pH values adequately. Ultrafast modulations near delay time zero can be observed in certain spectral ranges, e.g., in the transients at 627 nm for pH 6 and 595 nm for pH 9. These signals can be fitted by a time constant $\tau_1 < 200$ fs. Since this is within the temporal resolution of the experimental setup it cannot be ruled out that parts of the initial dynamics may be included in the cross-correlation function implicitly contained in the global fitting procedure. This leads to an increased uncertainty in the absolute value and the spectral properties of τ_1. Thus, only the amplitude spectrum for the subsequent kinetic components are shown (Figure 4) and included in the further analysis. The corresponding decay times τ_2, τ_3, and τ_4 are sufficient to describe the early events in the photocycle of PR up to 1 ns. Table 1 provides a summary of the obtained time constants at acidic and alkaline pH.

DISCUSSION

In the following section, two main aspects of the photocycle in PR on an ultrafast time scale will be addressed. The general features of the primary photoreaction are discussed first, followed by an explanation of the pH dependence of these events. The experiments provide information about the electronic response of the retinal chromophore after photoexcitation with a femtosecond time resolution. The time window of the acquired data (> 100 fs to 1 ns) allows for a detailed analysis of the photocycle of PR including the initial kinetics of the retinal isomerization and the impact of its direct molecular surroundings. The transient spectra for alkaline and acidic pH qualitatively display similar properties (Figure 2). Therefore, the following general description of the initial photoreaction should apply to both sample preparations.

Simultaneously with the pump pulse a positive signal builds up and decays within about 200 fs (Figure 2). This initial event is likely to constitute a part of the excited state dynamics of retinal in PR. In different retinal proteins, this signal has been attributed to the motion of the initially prepared wave packet out of the Franck−Condon region and resembles molecular conformational dynamics in the excited state (*11*, *17*, *20*).

The dominant positive feature in the blue spectral region can be assigned to excited state absorption, which in BR is observed at 460 nm. Its decay reflects the excited-to-ground-state transition. Time constants for the excited-state-to-ground-state transition of retinal in BR have been reported to occur extremely fast in about 500 fs (*17*, *33*). Similar to our observations for PR, excited state absorption at early delay times is also reported red shifted from the ground-state absorption maximum in BR (*34*).

At pH 6, the overall amplitude of the initial absorption is decreased and the spectral signature is red shifted. Parts of

the initial absorption signal (predominantly between 550 and 600 nm) may be superimposed by negative contributions that emerge on the same time scale. They arise both from stimulated emission, which is expected to be red shifted to the excitation wavelength, and from ground-state depopulation.

At longer delay times, excited state decay facilitates the observation of ground-state bleaching. Thus, negative signals clearly appear on the picosecond time scale between 450 and 500 nm. The depopulation of the ground state should also contribute at wavelengths longer than 550 nm, but these signals are overcompensated by strong positive absorption in this spectral region. Amplitude spectra suggest that both time constants denoted as τ_2 and τ_3 are involved in the decay of the prominent positive feature around 460 nm and the negative signals at the red end of the spectra around 700 nm. We thus observe a biphasic transition from the excited electronic state to the first ground-state product, represented by the decay of excited-state absorption and stimulated emission signals. This biexponential S_1-decay is commonly found in archaeal rhodopsins and even observed in protonated Schiff base retinal molecules in solution (*24*, *35*).

As the initial transient absorbance changes disappear several other signals build up at the same time scale. The S_1 decay leads to a long persisting positive absorption around 600 nm. This red-shifted absorption band is typical for the earliest photointermediates in the electronic ground state of several retinal proteins (*7*, *9*, *11*, *25*, *34*). It increases with time constants τ_2 and τ_3 as the excited state decays. On the contrary, amplitude spectra (Figure 4) of τ_3 indicate an absorption signal decrease around 650 nm. This can be explained by formation of ground-state intermediates on the same time scale. The photoproduct band may contain two different states, J and K (as described in BR), where J is a less red-shifted state and the J to K transition occurs on the time scale of a few picoseconds. The amplitude spectra of the long time offset τ_4 shows the expected features of the bleached ground state and the early K-type photoproduct.

In BR the first ground-state intermediate J converts with a time constant of 3 ps to the K intermediate (*18*). In the case of PR, the introduction of an additional picosecond time constant did not increase the quality of the global fit analysis. Thus, no statement with regard to a possible J to K transition can be made. However, our data support the assumption that the isomerization proceeds at the electronic ground state: the retinal either reaches the 13-cis configuration or relaxes back to *all-trans*. Since the latter causes an increasing ground-state population, this additional absorption may lead to the observed slight blue shift of the positive transient absorption band at longer delay times. The spectral changes observed for τ_2 and τ_3 in the corresponding range of their amplitude spectra (Figure 4) suggest a different quantum efficiency for photoisomerization for the fast (τ_2) and slow (τ_3) processes, i.e., for the different reaction pathways.

The existence of two time constants for the excited-state decay has to be considered in a reaction model consistent with the experimental findings. In general, two reasons can be responsible for biphasic excited-state kinetics:

(i) *Sample heterogeneity:* Here, the sample consists of at least two different species with different spectral properties and dynamic behavior. The retinal isomer composition in PR samples is the most likely candidate to cause sample heterogeneities of that kind. In the electronic ground-state PR contains retinal in both *all-trans* and 13-*cis* configurations. The amount of each isomer depends on the pH value and on the light conditions the sample is kept at (light- vs dark-adapted states). It was shown by retinal extraction experiments that PR at both pH values and adaptation states contains substantial amounts (≥ 20%) of 13-*cis* isomers (*7*). Because of its similar spectral properties and extinction coefficients, this species is also photoexcited, and it thus cannot be ruled out that it contributes to the observed transient absorbance signals.

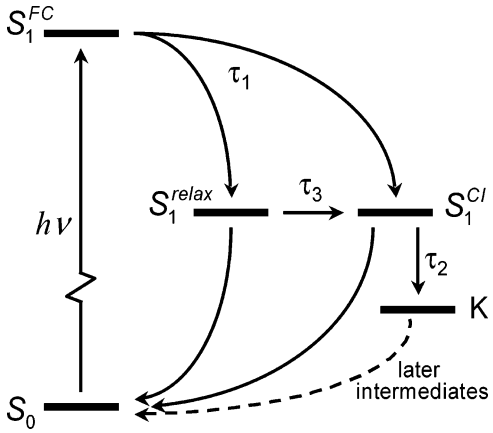

FIGURE 5: Energy level diagram and reaction scheme for the primary steps of the PR photocycle. S_0 and S_1 denote the ground and photoexcited state, respectively. Superscripts are used to illustrate the molecular motion along the S_1-potential energy surface: from the initially populated Franck−Condon region (FC) isomerization can proceed either directly via a conical intersection (CI) or via a longer lived S_1-state (relax). Time constants τ_1, τ_2, and τ_3 correspond to the values given in Table 1.

(ii) *Branched reaction model for a homogeneous sample:* The assumption of different reaction pathways in the excited state as previously suggested, for example, for retinal isomerization in halorhodopsin (HR) (*36*) allows us to describe the experimental findings for PR consistently (Figure 5). The initial motion along a certain coordinate (presumably involving both C−C stretching and torsional modes) (*37*−*39*) allows a fast transition to the ground state via a conical intersection (CI) as illustrated by the fast onset of a red-shifted product state absorption. The states decaying with the longer time constant τ_3 are not identical with the original Franck−Condon state. They may be reached by different initial motions and can access the CI region only within a few picoseconds.

The observation of two but significantly slower time constants for the acidic sample (pH < 7, Figure 3) allows discussing the role of the protonation status of the primary proton acceptor Asp97 on the photoisomerization rate of retinal: The first exited electronic state of retinal proteins is assumed to exhibit ionic (B_u-like) character. With respect to the charge distribution of the electronic ground state partial positive charge is moved toward the hydrocarbon tail of the chromophore upon excitation. This positive charge is stabilized by the negatively charged residues of Asp97 and Asp227 near the C13 position of the retinal and decreases the double bond character at this position. Accordingly, the energy required for the torsional motion, which might begin on the exited state surface, is lowered. As Asp97 is protonated at low pH, the energy required for the torsional

movement around the C13−C14 bond is increased, which is reflected in a slower reaction rate (*33*). The major importance of the negative charge at Asp97 for a fast subpicosecond photoproduct formation in PR is supported by similar findings in archaeal rhodopsins with uncharged residues at the Asp97 analogous position: acid purple BR samples (at pH < 2) or the BR D85N mutant as well as SR I show significantly slower reaction dynamics for the primary steps of the photocycle (*11*).

CONCLUSION

The ultrafast spectroscopic analysis of the earliest photoreactions places PR in a line with the ion pumping retinal proteins BR and HR and their mutants. The pH dependence of the initial dynamics underlines that speed and efficiency of the primary reactions are controlled by the charge distribution in the vicinity of the Schiff base.

The experimental observations can be compared to transient spectroscopy data on the ultrafast time scale of class I retinal proteins (BR, HR, SR I, and SR II) (*11*, *20*, *33*, *34*, *36*, *40*−*44*) and summarized as follows:

(i) An early response on a time scale of several tens or few hundreds of femtoseconds, although this may not occur before the following dynamics and at the same spectral position as described for PR. For PR, we attribute it to an initial wave packet-like motion out of the Franck−Condon region.

(ii) An absorption increase at about 400 to 500 nm, which originates from excited-state absorption. Decay of this component can be described by two time constants. Sensory rhodopsin might be an exception because its excited-state absorption was reported to be red shifted with respect to the other retinal proteins and its decay is well described by a single exponential (*11*).

(iii) Formation of a red-shifted photoproduct with hundreds of picoseconds to several nanoseconds lifetime at wavelengths around 600 nm.

Although there is no commonly accepted unifying model for the earliest events after light absorption in retinal proteins without inconsistencies, simple comparison of the spectral and dynamic features of the bacterial PR to the archaeal retinal proteins suggests that their ultrafast dynamics are highly related. This observation is interesting in respect to the different biological functions of the type I retinal proteins, which range from the ion pumps BR (proton transport) and HR (chloride transport) to the photosensors SR I and SR II. The details of the tuning mechanism still need to be related to the close environment of the Schiff base and the first (fast) reactions after light absorption.

REFERENCES

1. Beja, O., Aravind, L., Koonin, E. V., Suzuki, M. T., Hadd, A., Nguyen, L. P., Jovanovich, S., Gates, C. M., Feldman, R. A., Spudich, J. L., Spudich, E. N., and DeLong, E. F. (2000) Bacterial rhodopsin: Evidence for a new type of phototrophy in the sea, *Science 289*, 1902−1906.
2. Beja, O., Spudich, E. N., Spudich, J. L., Leclerc, M., and DeLong, E. F. (2001) Proteorhodopsin phototrophy in the ocean, *Nature 411*, 786−789.
3. de la Torre, J. R., Christianson, L. M., Beja, O., Suzuki, M. T., Karl, D. M., Heidelberg, J., and DeLong, E. F. (2003) Proteorhodopsin genes are distributed among divergent marine bacterial taxa, *Proc. Natl. Acad. Sci. U.S.A. 100*, 12830−12835.
4. Sabehi, G., Massana, R., Bielawski, J. P., Rosenberg, M., Delong, E. F., and Beja, O. (2003) Novel proteorhodopsin variants from the Mediterranean and Red Seas, *Environ. Microbiol. 5*, 842−849.
5. Venter, J. C., Remington, K., Heidelberg, J. F., Halpern, A. L., Rusch, D., Eisen, J. A., Wu, D. Y., Paulsen, I., Nelson, K. E., Nelson, W., Fouts, D. E., Levy, S., Knap, A. H., Lomas, M. W., Nealson, K., White, O., Peterson, J., Hoffman, J., Parsons, R., Baden-Tillson, H., Pfannkoch, C., Rogers, Y. H., and Smith, H. O. (2004) Environmental genome shotgun sequencing of the Sargasso Sea, *Science 304*, 66−74.
6. Krebs, R. A., DeVita, A. M., Parthasarathy, R., Alexiev, U., Dunmire, D., and Braiman, M. S. (2002) Purification and spectroscopic studies of proteorhodopsin, *Biophys. J. 82*, 224A−224A.
7. Friedrich, T., Geibel, S., Kalmbach, R., Chizhov, I., Ataka, K., Heberle, J., Engelhard, M., and Bamberg, E. (2002) Proteorhodopsin is a light-driven proton pump with variable vectoriality, *J. Mol. Biol. 321*, 821−838.
8. Dioumaev, A. K., Brown, L. S., Shih, J., Spudich, E. N., Spudich, J. L., and Lanyi, J. K. (2002) Proton transfers in the photochemical reaction cycle of proteorhodopsin, *Biochemistry 41*, 5348−5358.
9. Varo, G., Brown, L. S., Lakatos, M., and Lanyi, J. K. (2003) Characterization of the photochemical reaction cycle of proteorhodopsin, *Biophys. J. 84*, 1202−1207.
10. Lakatos, M., Lanyi, J. K., Szakacs, J., and Varo, G. (2003) The photochemical reaction cycle of proteorhodopsin at low pH, *Biophys. J. 84*, 3252−3256.
11. Lutz, I., Sieg, A., Wegener, A. A., Engelhard, M., Boche, I., Otsuka, M., Oesterhelt, D., Wachtveitl, J., and Zinth, W. (2001) Primary reactions of sensory rhodopsins, *Proc. Natl. Acad. Sci. U.S.A. 98*, 962−967.
12. Krebs, R. A., Dunmire, D., Partha, R., and Braiman, M. S. (2003) Resonance Raman characterization of proteorhodopsin's chromophore environment, *J. Phys. Chem. B 107*, 7877−7883.
13. Dioumaev, A. K., Richter, H. T., Brown, L. S., Tanio, M., Tuzi, S., Saito, H., Kimura, Y., Needleman, R., and Lanyi, J. K. (1998) Existence of a proton-transfer chain in bacteriorhodopsin: Participation of Glu-194 in the release of protons to the extracellular surface, *Biochemistry 37*, 2496−2506.
14. Balashov, S. P., Imasheva, E. S., Ebrey, T. G., Chen, N., Menick, D. R., and Crouch, R. K. (1997) Glutamate-194 to cysteine mutation inhibits fast light-induced proton release in bacteriorhodopsin, *Biochemistry 36*, 8671−8676.
15. Brown, L. S., Sasaki, J., Kandori, H., Maeda, A., Needleman, R., and Lanyi, J. K. (1995) Glutamic-Acid-204 Is the Terminal Proton Release Group at the Extracellular Surface of Bacteriorhodopsin, *J. Biol. Chem. 270*, 27122−27126.
16. Dioumaev, A. K., Wang, J. M., Balint, Z., Varo, G., and Lanyi, J. K. (2003) Proton transport by proteorhodopsin requires that the retinal Schiff base counterion Asp-97 be anionic, *Biochemistry 42*, 6582−6587.
17. Mathies, R. A., Cruz, C. H. B., Pollard, W. T., and Shank, C. V. (1988) Direct Observation of the Femtosecond Excited-State Cis−Trans Isomerization in Bacteriorhodopsin, *Science 240*, 777−779.
18. Herbst, J., Heyne, K., and Diller, R. (2002) Femtosecond infrared spectroscopy of bacteriorhodopsin chromophore isomerization, *Science 297*, 822−825.
19. Petrich, J. W., Breton, J., Martin, J. L., and Antonetti, A. (1987) Femtosecond Absorption-Spectroscopy of Light-Adapted and Dark-Adapted Bacteriorhodopsin, *Chem. Phys. Lett. 137*, 369−375.
20. Dobler, J., Zinth, W., Kaiser, W., and Oesterhelt, D. (1988) Excited-State Reaction Dynamics of Bacteriorhodopsin Studied by Femtosecond Spectroscopy, *Chem. Phys. Lett. 144*, 215−220.
21. Atkinson, G. H., Ujj, L., and Zhou, Y. D. (2000) Vibrational spectrum of the J-625 intermediate in the room-temperature bacteriorhodopsin photocycle, *J. Phys. Chem. A 104*, 4130−4139.
22. Song, L., and El-Sayed, M. A. (1998) Primary step in bacteriorhodopsin photosynthesis: Bond stretch rather than angle twist of its retinal excited-state structure, *J. Am. Chem. Soc. 120*, 8889−8890.
23. Garavelli, M., Celani, P., Bernardi, F., Robb, M. A., and Olivucci, M. (1997) The $C_5H_6NH^{2+}$ protonated Shiff base: An ab initio minimal model for retinal photoisomerization, *J. Am. Chem. Soc. 119*, 6891−6901.
24. Hamm, P., Zurek, M., Roschinger, T., Patzelt, H., Oesterhelt, D., and Zinth, W. (1996) Femtosecond spectroscopy of the photo-

isomerisation of the protonated Schiff base of all-trans retinal, *Chem. Phys. Lett. 263*, 613−621.
25. Oesterhelt, D. (1998) The structure and mechanism of the family of retinal proteins from halophilic archaea, *Curr. Opin. Struct. Biol. 8*, 489−500.
26. Honig, B., Dinur, U., Nakanishi, K., Baloghnair, V., Gawinowicz, M. A., Arnaboldi, M., and Motto, M. G. (1979) External Point-Charge Model for Wavelength Regulation in Visual Pigments, *J. Am. Chem. Soc. 101*, 7084−7086.
27. Tajkhorshid, E., and Suhai, S. (1999) The effect of the protein environment on the structure and charge distribution of the retinal Schiff base in bacteriorhodopsin, *Theor. Chem. Acc. 101*, 180−185.
28. Torii, H. (2002) Vibrational polarization and opsin shift of retinal Schiff bases: Theoretical study, *J. Am. Chem. Soc. 124*, 9272−9277.
29. Luecke, H., Schobert, B., Richter, H. T., Cartailler, J. P., and Lanyi, J. K. (1999) Structure of bacteriorhodopsin at 1.55 angstrom resolution, *J. Mol. Biol. 291*, 899−911.
30. Imasheva, E. S., Balashov, S. P., Wang, J. M., Dioumaev, A. K., and Lanyi, J. K. (2004) Selectivity of retinal photoisomerization in proteorhodopsin is controlled by aspartic acid 227, *Biochemistry 43*, 1648−1655.
31. Kovalenko, S. A., Dobryakov, A. L., Ruthmann, J., and Ernsting, N. P. (1999) Femtosecond spectroscopy of condensed phases with chirped supercontinuum probing, *Phys. Rev. A 59*, 2369−2384.
32. Balashov, S. P., Imasheva, E. S., Govindjee, R., and Ebrey, T. G. (1991) Quantum Yield Ratio of the Forward and Back Light Reactions of Bacteriorhodopsin at Low-Temperature and Photosteady-State Concentration of the Bathoproduct-K, *Photochem. Photobiol. 54*, 955−961.
33. Song, L., El-Sayed, M. A., and Lanyi, J. K. (1993) Protein Catalysis of the Retinal Subpicosecond Photoisomerisation in the Primary Process of Bacteriorhodopsin Photosynthesis, *Science 261*, 891−894.
34. Hasson, K. C., Gai, F., and Anfinrud, P. A. (1996) The photoisomerization of retinal in bacteriorhodopsin: Experimental evidence for a three-state model, *Proc. Natl. Acad. Sci. U.S.A. 93*, 15124−15129.
35. Hou, B., Friedman, N., Ruhman, S., Sheves, M., and Ottolenghi, M. (2001) Ultrafast spectroscopy of the protonated Schiff bases of free and C-13=C-14 locked retinals, *J. Phys. Chem. B 105*, 7042−7048.
36. Arlt, T., Schmidt, S., Zinth, W., Haupts, U., and Oesterhelt, D. (1995) The Initial Reaction Dynamics of the Light-Driven Chloride Pump Halorhodopsin, *Chem. Phys. Lett. 241*, 559−565.
37. Kobayashi, T., Saito, T., and Ohtani, H. (2001) Real-time spectroscopy of transition states in bacteriorhodopsin during retinal isomerization, *Nature 414*, 531−534.
38. Schoenlein, R. W., Peteanu, L. A., Mathies, R. A., and Shank, C. V. (1991) The 1st Step in Vision − Femtosecond Isomerization of Rhodopsin, *Science 254*, 412−415.
39. Ye, T., Gershgoren, E., Friedman, N., Ottolenghi, M., Sheves, M., and Ruhman, S. (1999) Resolving the primary dynamics of bacteriorhodopsin, and of a 'C-13=C-14 locked' analog, in the reactive excited state, *Chem. Phys. Lett. 314*, 429−434.
40. Gai, F., Hasson, K. C., McDonald, J. C., and Anfinrud, P. A. (1998) Chemical dynamics in proteins: The photoisomerization of retinal in bacteriorhodopsin, *Science 279*, 1886−1891.
41. Logunov, S. L., El-Sayed, M. A., Song, L., and Lanyi, J. K. (1996) Photoisomerization quantum yield and apparent energy content of the K intermediate in the photocycles of bacteriorhodopsin, its mutants D85N, R82Q, and D212N, and deionized blue bacteriorhodopsin, *J. Phys. Chem. 100*, 2391−2398.
42. Haacke, S., Schenkl, S., Vinzani, S., and Chergui, M. (2002) Femtosecond and picosecond fluorescence of native bacteriorhodopsin and a nonisomerizing analog, *Biopolymers 67*, 306−309.
43. Kennis, J. T. M., Larsen, D. S., Ohta, K., Facciotti, M. T., Glaeser, R. M., and Fleming, G. R. (2002) Ultrafast protein dynamics of bacteriorhodopsin probed by photon echo and transient absorption spectroscopy, *J. Phys. Chem. B 106*, 6067−6080.
44. Du, M., and Fleming, G. R. (1993) Femtosecond Time-Resolved Fluorescence Spectroscopy of Bacteriorhodopsin − Direct Observation of Excited-State Dynamics in the Primary Step of the Proton Pump Cycle, *Biophys. Chem. 48*, 101−111.

BI048318H